Journal of Thermal Analysis and Calorimetry (2020) 140:2293–2303
https://doi.org/10.1007/s10973-019-08958-3

Mechanochemical synthesis, characterization and thermal study of new cocrystals of ciprofloxacin with pyrazinoic acid and *p*-aminobenzoic acid

Amanda Cosmo de Almeida[1] · Patrícia Osório Ferreira[1] · Carolina Torquetti[2] · Bruno Ekawa[1] · Ana Carina Sobral Carvalho[1] · Everton Carvalho dos Santos[2] · Flávio Junior Caires[1,2]

Received: 25 May 2019 / Accepted: 25 October 2019 / Published online: 6 November 2019

Abstract
Novel cocrystals of ciprofloxacin with pyrazinoic acid and *p*-aminobenzoic acid in the 1:1 stoichiometric ratio were obtained by the mechanochemical method, under conditions of liquid-assisted grinding (LAG/ethanol) and neat grinding. They were characterized by powder X-ray diffractometry, infrared spectroscopy, simultaneous thermogravimetry, differential thermal analysis, differential scanning calorimetry (DSC) and DSC-Microscopy system. The results confirmed the successful synthesis of the cocrystals and indicated the functional groups responsible for the formation of the new supramolecular synthons. In addition, from the thermal analysis, it was possible to evaluate the thermal stability, composition, crystallization processes during heating, polymorphic transitions and construct the binary phase diagrams.

Keywords Cocrystal · Ciprofloxacin · Mechanochemical synthesis · Thermal analysis

Introduction

In the pharmaceutical industry, enhancing the essential properties of an active pharmaceutical ingredient (API), i.e., aqueous solubility and bioavailability, without compromising therapeutic efficacy is one of the major challenges faced in the discovery and development of a new drug [1–4]. Solid forms, such as cocrystals and salts, are approaches potentially used to improve the physicochemical properties of APIs [4–10]. Pharmaceutical cocrystals can be defined as multicomponent crystalline compounds, containing an API and one or more cocrystal formers (coformers), in a definite stoichiometric ratio, linked by intermolecular interactions, such as hydrogen bonds. Usually, in the formation of a cocrystal, both components are in the solid state and non-ionic species at ambient conditions [3, 10–12].

Ciprofloxacin (CIP; $C_{17}H_{18}FN_3O_3$), shown in Fig. 1a, is a broad-spectrum bioactive agent widely used in the treatment of bacterial infections, acting primarily on DNA-gyrase and inhibition of topoisomerase IV. Thus, CIP is approved for the treatment of 14 types of infections, especially in the urinary tract [13–16]. Its aqueous solubility is strongly pH dependent due to the formation of zwitterionic species resulting from the protons transfer of the carboxylic acid to the basic piperazine ring. Such dependence generates low solubility at neutral pH, limiting the bioavailability of the compound. In addition, CIP has low permeability across biological membranes. As a result, such API is a class IV drug in the Biopharmaceutical Classification System (BCS) [17, 18]. In the literature, some studies have reported the formation of CIP salts and cocrystals, showing improvements in the physicochemical properties of this API, especially in its solubility, as we have previously reported that the CIP cocrystals with nicotinic and isonicotinic acids could show a 20-fold increase in solubility of both compounds [17–21].

To form a pharmaceutical cocrystal, at least a second compound is needed in addition to the API. Frequently, such additional compound is chosen among pharmaceutically acceptable molecules or from the "generally recognized as

Electronic supplementary material The online version of this article (https://doi.org/10.1007/s10973-019-08958-3) contains supplementary material, which is available to authorized users.

✉ Flávio Junior Caires
flavio.caires@unesp.br

[1] Institute of Chemistry, São Paulo State University (UNESP), Araraquara, Brazil

[2] School of Sciences, São Paulo State University (UNESP), Bauru, Brazil

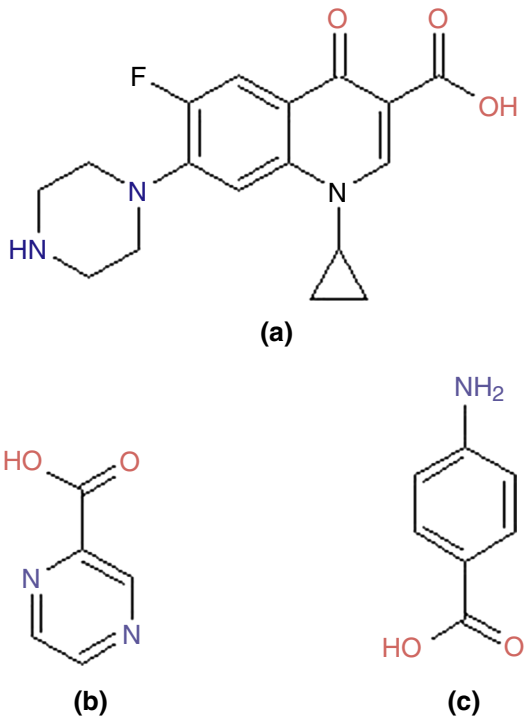

Fig. 1 Structural formula of ciprofloxacin drug (**a**), pyrazinoic acid (**b**) and *p*-aminobenzoic acid (**c**)

safe" (GRAS) list, such as flavonoids, nutraceuticals, vitamins, minerals, food additives, preservatives, excipients, amino acids, biomolecules and other APIs [22–26]. In the present, pyrazinoic acid (PZCA; $C_5H_4N_2O_2$) and *p*-aminobenzoic acid (PABA; $C_7H_7NO_2$) were chosen as coformer.

Pyrazinoic acid or pyrazine-2-carboxylic acid, shown in Fig. 1b, is the product of the bioconversion of pyrazinamide by the enzyme pyrazinamidase, which is considered the active form with activity against *Mycobacterium tuberculosis* [27–29]. This acid is commercially available, stable, soluble in water and exhibits a rich coordination chemistry, being widely used in the preparation of different metal complexes, coordination polymers or metal–organic structures [27, 29, 30]. It has a molar mass of 124.10 g mol^{-1}, and its structure is composed of carboxylic acid and pyridine groups, which enable the formation of salts and cocrystals, as reported by Drozd et al. [31] and Prasad et al. [32], respectively.

The 4-aminobenzoic acid or *p*-aminobenzoic acid, shown in Fig. 1c, is a white-yellowish solid having molar mass equal to 137.14 g mol^{-1} [33]. Also known as vitamin B_{10}, this compound is not synthesized by the human body, but can be found in food, such as grains, eggs, milk and meat. In addition to being used as an anti-inflammatory, antibacterial, anticoagulant agent and UV radiation blocker, in the human body, PABA is necessary for the synthesis of folic acid [33–36]. Moreover, such compound has been used in many studies mostly because of its pharmaceutical properties and ability to form multicomponent solid forms, which is attributed mainly to the amine and carboxyl functional groups capable of forming hydrogen bonds [31, 37, 38].

This study reports the synthesis of new multicomponent solids of ciprofloxacin with pyrazinoic acid and *p*-aminobenzoic acid using the mechanochemical method in neat grinding (NG) and liquid-assisted grinding (LAG) conditions. The characterization was performed using infrared (FTIR) spectroscopy and powder X-ray diffractometry (PXRD) to confirm the synthesis of the new cocrystals and to infer the probable sites of interaction between the molecules. In addition, to determine the thermal properties of the compounds obtained, a thorough thermoanalytical study was performed using thermogravimetry–differential thermal analysis (TG–DTA), differential scanning calorimetry (DSC) and DSC-Microscopy. Finally, the binary phase diagram of these systems was constructed to confirm the stoichiometry of the prepared cocrystals.

Experimental part

Materials

Ciprofloxacin (CIP, 98% purity), pyrazinoic acid (PZCA, 99% purity) and 4-aminobenzoic acid (PABA, 99% purity) were obtained from Sigma-Aldrich and used as received. Additionally, the solvent used during the LAG was the ethanol (EtOH, 99.5% purity), purchased from Dinâmica.

Mechanochemical synthesis

The mechanochemical synthesis of the new multicomponent solid forms of CIP with PZCA and PABA was carried out in a Retsch ball mill, model MM400, using steel grinding jars of 10 mL volume and one stainless steel grinding ball of 7 mm diameter.

The neat grinding (NG) and liquid-assisted grinding (LAG) using ethanol as solvent were carried out in a 1:1 molar ratio between the drug and the coformers, at the grinding frequency of 15 and 30 Hz with total sample mass of 100 and 500 mg, respectively. The amount of solvent added in the synthesis was calculated from the 0.25 µL mg^{-1} ratio (volume/total sample mass), as determined by Friscic et al. [39]. The conditions of synthesis and the quantity of precursors used in the cocrystal preparation are presented in Table 1.

After the synthesis, the material was maintained at 50 °C for 24 h in a forced air circulation oven and stored in a glass desiccator containing anhydrous calcium chloride until the analyses.

Table 1 Conditions chosen to synthesize the CIP cocrystals

Systems	Total mass/mg	API: coformer mass/mg	Synthesis time/min	Frequency/Hz	Ethanol volume/μL
CIP–PZCA	500	363.76: 134.24	30	30	125
					0
	100	72.75: 27.25		15	25
					0
CIP–PABA	500	353.63: 146.37		30	125
					0
	100	70.73: 29.27		15	25
					0

Equipment

Powder X-ray diffractograms were obtained from Rigaku MiniFlex model using the CuKα radiation of a copper tube ($\lambda = 1.54056$ Å), subjected to 40 kV, 15 mA current. The angular experimental range was $5 \leq 2\theta \leq 50°$.

Infrared (FTIR) spectra were obtained on the Thermo Scientific spectrometer, Nicolet iS10, using the germanium crystal attenuated total reflectance method, in the wavelength range of 675 to 4000 cm^{-1}, with the resolution of 4 cm^{-1} and 32 scans per spectrum.

The DSC curves were obtained in an equipment of TA Instruments, model Q10, using closed aluminum crucible of 40 μL (sample and reference) with lids with a pinhole in the center, sample mass of 2.5 mg, heating rate of 10 °C min^{-1} and dynamic air atmosphere with flow rate of 50 mL min^{-1}. To obtain the DSC curve of pure pyrazinoic acid, a sealed aluminum crucible was used, because the sample completely sublimated before melting.

The DSC-Microscopy system analysis was obtained using a Mettler Toledo DSC 1 STARe system coupled to an OLYMPUS digital camera, model SC 30, which incorporates a 3.3-megapixel CMOS sensor and an optical subassembly mechanic Navitar 1-6232D with 6.5X zoom. The experimental conditions were similar to those used to obtain the DSC curves, except that an uncovered α-alumina crucible was used.

The TG–DTA analysis was done using an equipment of TA Instruments, model SDT 2960. The curves were obtained in α-Al_2O_3 crucible (70 μL), with sample mass of approximately 5.0 mg, heating rate of 10 °C min^{-1}, dynamic air atmosphere with flow rate of 50 mL min^{-1} and temperature range of 30–800 °C.

Finally, the experimental binary phase diagram for these systems was constructed from the extrapolated temperatures (T_{onset}) of the first melting peak and the peak temperatures (T_p) of the last melt peak observed in the DSC curve (total sample melt) [2, 40]. These temperatures were obtained from the DSC curves of the mixtures of ciprofloxacin with PABA and PZCA in the molar fractions of 0, 0.25, 0.33, 0.5, 0.66, 0.75 and 1.0.

Results and discussion

CIP–PZCA (1:1) system

PXRD and FTIR spectroscopy

The PXRD diffractograms and the FTIR spectra of the cocrystal and the isolated components are shown in Fig. 2.

The diffractograms of this system differ significantly from those obtained from its precursors. The CIP–PZCA systems synthesized at 15 Hz (NG and LAG) and the system prepared at 30 Hz (NG) show a diffraction pattern very similar to each other, although the latter showed amorphization during the mechanochemical synthesis [41], as suggested by the diffraction halo in its diffractogram. These samples have new diffraction peaks in 2θ equal to 5.5°, 18.9°, 26.4°, indicating the presence of a new crystalline phase, which is an evidence of the cocrystal formation.

For the CIP–PZCA/LAG (30 Hz) system, a distinct diffraction pattern is observed, with new peaks in 2θ equal to 5.5°, 10.8°, 11.5°, 15.0°, 18.9°, 19.5° and 26.0°, which suggests the obtention of another polymorph or polymorph mixture in this condition of synthesis, as already reported in other studies [42, 43].

The main FTIR assignments of CIP, PZCA and CIP–PZCA systems are shown in Table S1 (supplementary material). In the FTIR spectrum of CIP, the bands at 1589 cm^{-1} and 1375 cm^{-1} were observed and assigned to the asymmetric and symmetric stretching vibrations of the carboxylate group (ν_{asym} COO^- and ν_{sym} COO^-), respectively; the low intensity band in the region of 2580–2680 cm^{-1} was assigned to the stretching vibrations of the NH_2^+ group. These bands show evidence that in the solid state, CIP assumes zwitterionic form [15, 44]. In turn, the main bands observed in the infrared spectrum

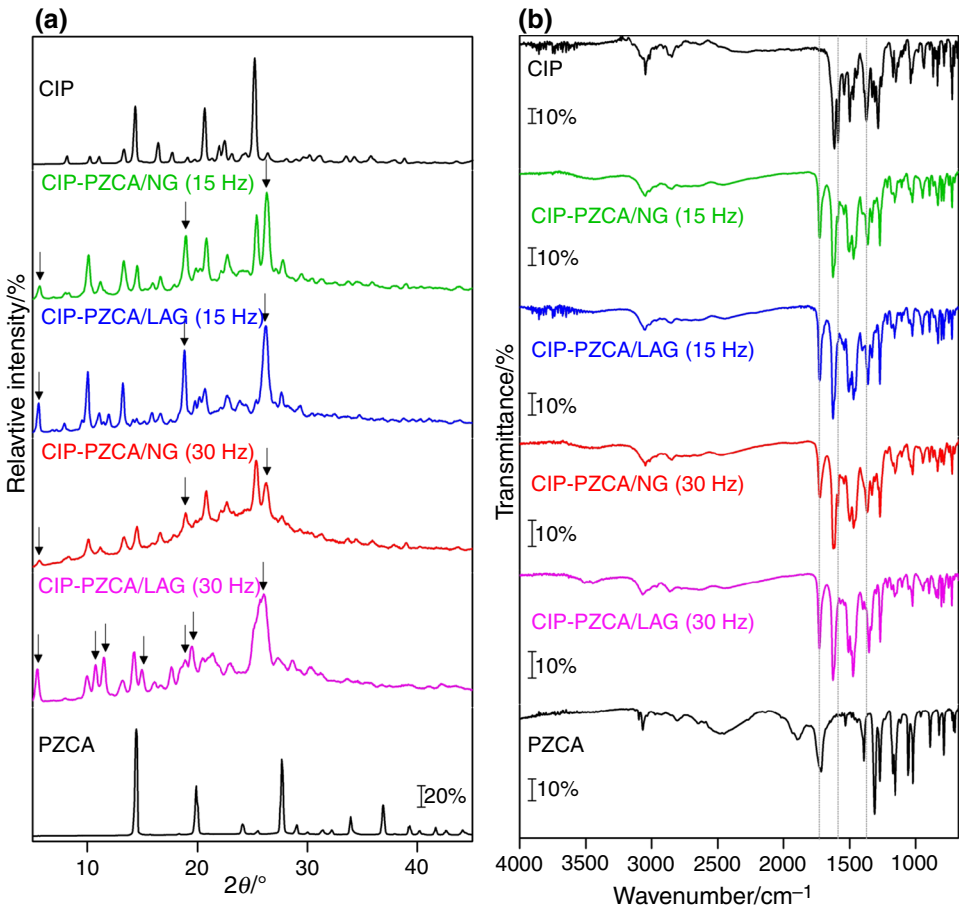

Fig. 2 PXRD diffractograms (**a**) and FTIR spectra (**b**) of the pure components and the CIP–PZCA systems

of PZCA are attributed to C=O stretching vibrations at 1715 cm^{-1} and the two broad bands around 2500 cm^{-1} and 1900 cm^{-1} are assigned to intermolecular hydrogen bonding OH···N between the carboxylic group and the aromatic nitrogen [29, 30].

The FTIR spectrum of the CIP–PZCA system shows significant changes in relation to the pure component spectrum, mainly the absence of the $\nu_{asym}COO^-$ and $\nu_{sym}COO^-$ of CIP and vibrations assigned to intermolecular hydrogen bonding OH···N between the molecules of PZCA. In addition, there is a hypsochromic shift of the absorption band attributed to νC=O of the carboxylic group of PZCA from 1715 to 1726 cm^{-1}. Also, in the spectra, a weak band at 3450 cm^{-1} is observed and attributed to νO–H, a slight shift of the band attributed to νC=O (ketone group) from 1616 to 1626 cm^{-1}, as well as the appearance of a broad band between 3200 and 2000 cm^{-1} attributed to νO–H superimposed on the νC–H bands. These changes in the spectra suggest the establishment of new supramolecular synthons, such as hydrogen acid–acid bonds, suggesting as well that these changes occurred due to the formation of a cocrystal rather than a salt.

TG–DTA and DSC analyses

The TG–DTA and DSC curves of the pure compounds and CIP–PZCA cocrystal are shown in Fig. 3a, b, respectively.

The thermoanalytical curves of CIP show that it melts at 270 °C, has thermal stability up to 280 °C and undergoes thermal decomposition in three overlapping steps, according to the recently reported results [19].

The TG–DTA curves show that pyrazinoic acid undergoes a total mass loss in a single step between 150 and 225° C, corresponding to the endothermic peak at 218 °C in the DTA curve. The compound was placed in a test tube and heated to 10 °C min^{-1} in a melting point apparatus, which showed that it sublimates and condenses on the walls of the tube, without undergoing thermal decomposition, as also confirmed by FTIR analyses of the material. The DSC curve (closed crucible) of pyrazinoic acid shows an endothermic

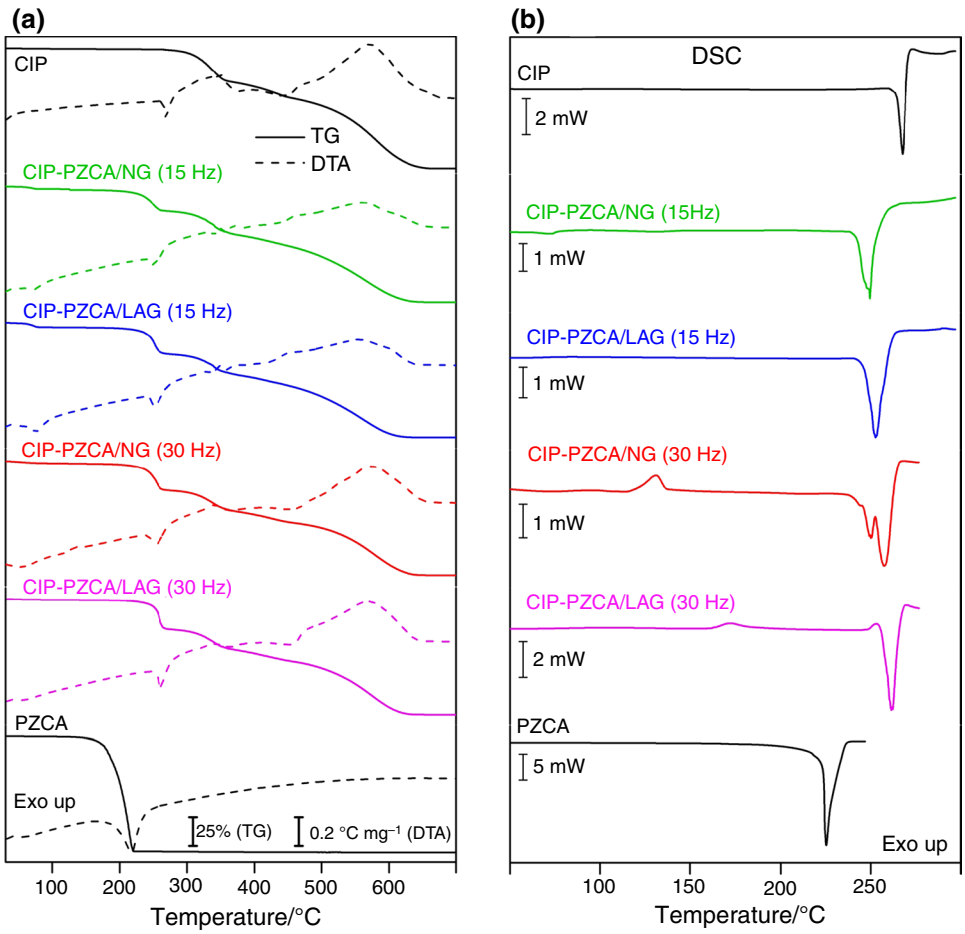

Fig. 3 TG–DTA (**a**) and DSC (**b**) curves of the pure compounds and the CIP–PZCA system

peak at 225 °C ($\Delta H_{fus} = 872.8$ J g^{-1}), attributed to the melting of the compound.

The TG–DTA curves of the CIP–PZCA (1:1) cocrystal show at least three overlapping mass loss steps in the TG curve and thermal stability of approximately 205 °C. The first step, between 205 and 265 °C, is attributed to the beginning of the thermal decomposition of the cocrystal with release of the coformer ($\Delta m_{Calc.} = 27.0\%$; $\Delta m_{TG} = 26.7\%$). The following two mass loss steps, corresponding to the endothermic and exothermic events in the DTA curve, are attributed to thermal degradation of the remaining drug. The endothermic peak at 252 °C (CIP–PZCA/NG or LAG (15 Hz)) or 261 °C (CIP–PZCA/LAG (30 Hz)) in the DSC curve is attributed to incongruent melting. In the DSC curve of the synthesized sample without addition of solvent (net grinding) at 30 Hz, two consecutive melting peaks (252 °C and 258 °C) are observed, which suggests a mixture of polymorphs.

The TG–DTA curves of both systems synthesized at 15 Hz (NG and LAG) show a small mass loss up to 80 °C, corresponding to a small endothermic peak in the DTA curve, and the subtle event present in the DSC curve is attributed to residual solvent elimination and/or water adsorbed by the samples.

The exothermic events at 130 °C (CIP–PZCA/NG (30 Hz)) and 172 °C (CIP–PZCA/LAG (30 Hz)) in the DSC curves were investigated in more detail by heating these samples to temperatures after these thermal events followed by the characterization by PXRD and FTIR spectroscopy as discussed in the next sections.

Study of the exothermic events in the DSC curves

The PXRD diffractograms and FTIR spectra of the heated CIP–PZCA/NG (30 Hz) cocrystal and of the cocrystal after 5 months of synthesis are shown in Fig. 4.

These diffractograms show that the diffraction halo disappears over time or when the sample is heated, increasing the intensity of the diffraction peaks. This suggests that

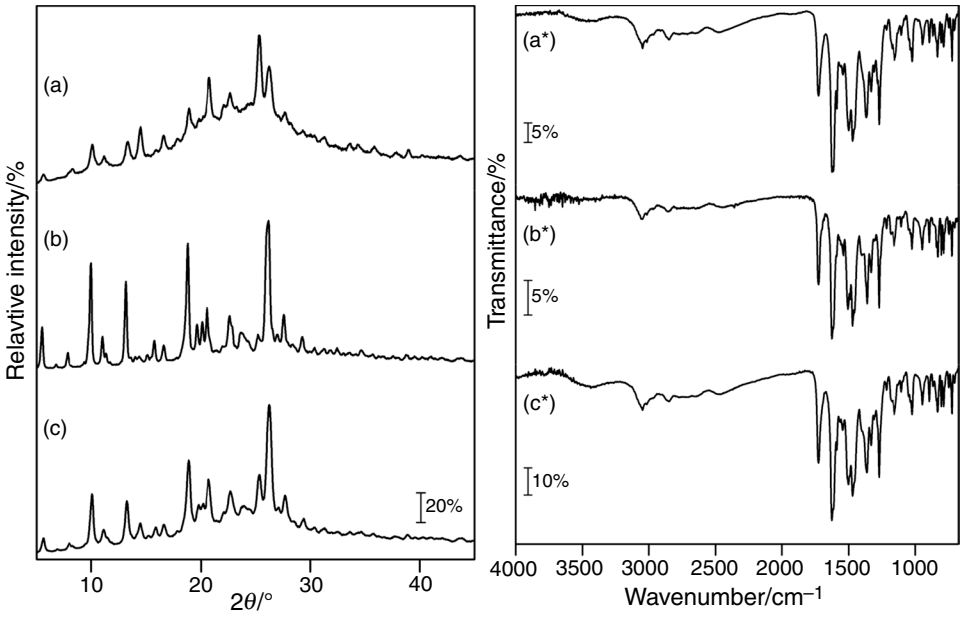

Fig. 4 PXRD diffractograms (**a**, **b** and **c**) and FTIR spectra (**a***, **b*** and **c***) of the CIP–PZCA/NG (30 Hz) cocrystal at 25 °C (**a** and **a***), heated up to 190 °C (**b** and **b***) and after 5 months of synthesis (**c** and **c***)

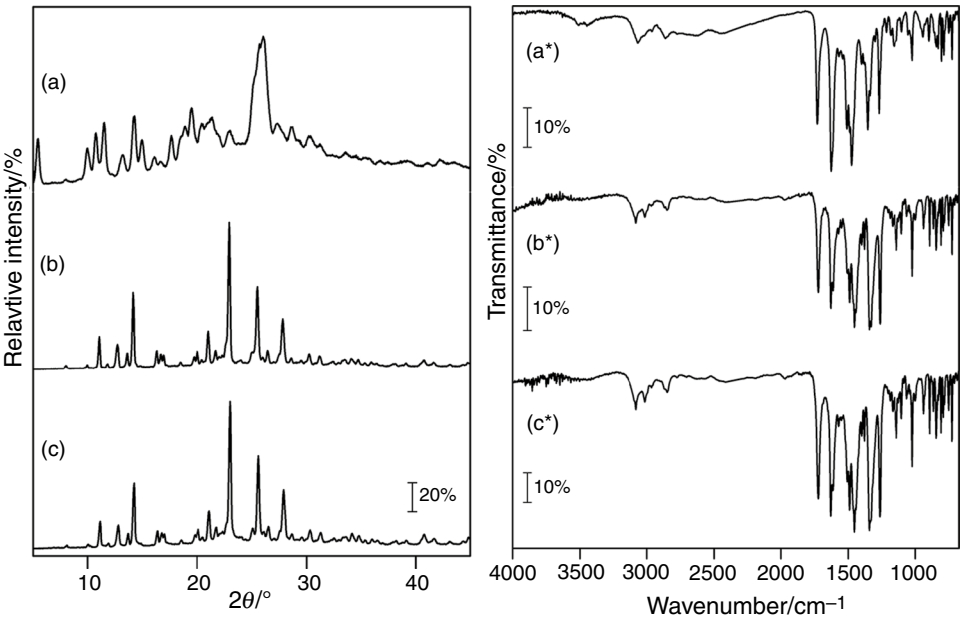

Fig. 5 PXRD diffractograms (**a**, **b** and **c**) and FTIR spectra (**a***, **b*** and **c***) of the CIP–PZCA/LAG (30 Hz) cocrystal at 25 °C (**a** and **a***), heated up to 205 °C (**b**, **b***) and after 5 months of synthesis (**c** and **c***)

the exothermic event present in the DSC curve is attributed to a crystallization process of the material, which is common in materials that undergo amorphization during grinding [41]. In addition, this thermal event almost disappears from the DSC curve obtained from the material after 5 months of synthesis (Fig. S1, supplementary material). The FTIR spectra confirm this interpretation, since the spectral pattern remains very similar, ruling out possible polymorphic transitions [45–47].

The PXRD diffractograms and FTIR spectra of the heated CIP–PZCA/LAG (30 Hz) cocrystal and of the cocrystal after 5 months of synthesis are shown in Fig. 5.

The diffractograms show that at a higher temperature than the exothermic event in the DSC curve and with time, a new diffraction pattern is observed in the sample. In addition, this thermal event disappears from the DSC curve obtained from the material after 5 months of synthesis (Fig. S2, supplementary material). This indicates that the exothermic

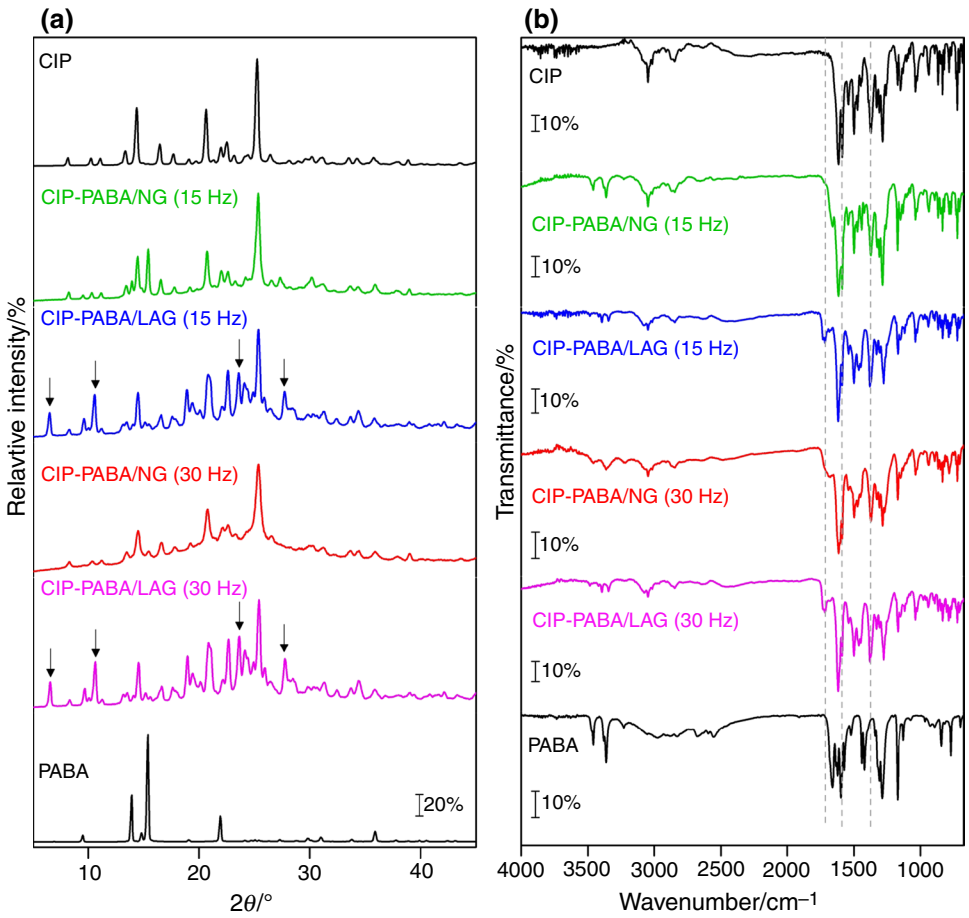

Fig. 6 PXRD diffractograms (**a**) and FTIR spectra (**b**) of the pure components and the CIP–PABA systems

event in the DSC curve refers to an irreversible crystalline phase transition, that is, a monotropy relationship between the polymorphs [48]. Moreover, changes in the FTIR spectra are observed, especially in the region between 3600 and 2000 cm^{-1}, probably due to changes in the intermolecular interactions in the solid state, which confirms this polymorphic transition [42, 43].

CIP–PABA (1:1) system

PXRD and FTIR spectroscopy

The PXRD diffractograms and the FTIR spectra of the CIP–PABA systems are presented in Fig. 6a, b, respectively.

The diffractograms of the systems prepared with ethanol addition (LAG) showed new peaks in 2θ equal to 6.5°; 9.6°; 23.5°; 27.6°, which confirms the formation of a new crystalline phase. This also shows that the liquid-assisted grinding (LAG) improved the formation reaction of the new material, as previously reported by other authors [39, 49]. The diffractograms of the systems obtained without addition of solvent (NG) did not present new diffraction peaks, being just the combination of the diffraction patterns of their pure precursors, suggesting that these systems are just a physical or eutectic mixture.

The main FTIR assignments of CIP–PABA systems and the precursors are shown in Table S2 (supplementary material). The FTIR spectrum of 4-aminobenzoic acid shows a band at 1662 cm^{-1} attributed to the C=O stretch (νC=O, –COOH group) and a broad band in the region of 3300–2200 cm^{-1} which overlaps with the C–H stretches (νC–H), attributed to the O–H stretch (νO–H, –COOH group). The two bands attributed to the N–H stretch (νN–H, NH_2 group) are also present at 3460 cm^{-1} and 3363 cm^{-1} [35, 50].

The FTIR spectra of the systems synthesized by the LAG method show a band shift assigned to νC=O (PABA) from 1662 to 1717 cm^{-1} ($\Delta\nu = 55$ cm^{-1}). This shift, however, is not very pronounced in the spectra of the samples synthesized by the NG method ($\Delta\nu = 0$ cm^{-1} for the 15 Hz sample and $\Delta\nu = 17$ cm^{-1} for the 30 Hz sample), showing only a

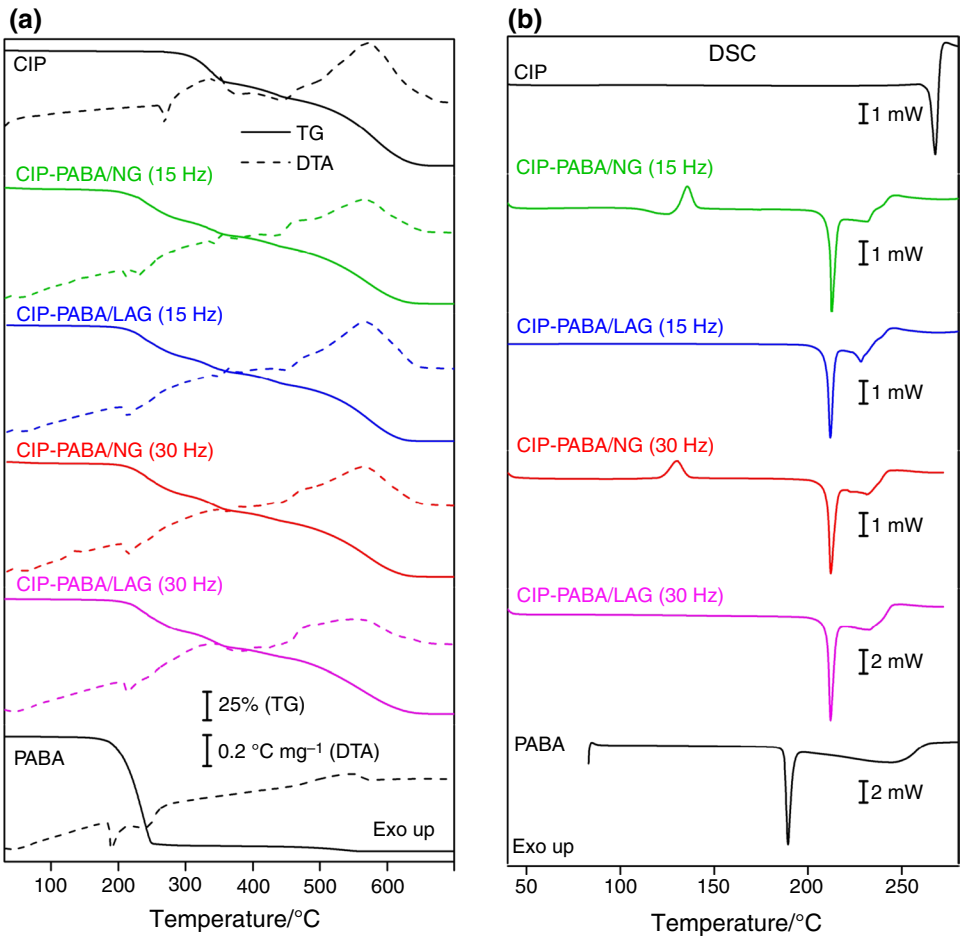

Fig. 7 TG-DTA (**a**) and DSC (**b**) curves of the pure compounds and the CIP–PABA system

combination of the spectra of its precursors. In addition, bands related to the carboxylate group of the drug were observed at 1590 cm^{-1} and 1380 cm^{-1} assigned to ν_{asym} (COO^-) and ν_{sym} (COO^-), respectively, indicating a cocrystal formation between the zwitterionic form of the drug with the coformer in the neutral form.

TG–DTA and DSC analyses

The TG–DTA and DSC curves of the system obtained between CIP and PABA are shown in Fig. 7a, b, respectively.

The TG–DTA curves show that the PABA is thermally stable up to 170 °C and presents two mass loss steps, corresponding to the endothermic event (240° C) and exothermic event (545 °C) in the DTA curve, respectively. These mass losses correspond to the partial evaporation and decomposition of the coformer, generating a carbonized residue that is oxidized slowly at higher temperatures [33]. The endothermic peak at 190 °C (DTA) and 189 °C (DSC), without significant mass loss in the TG curve, corresponds to the melting of the coformer.

For CIP–PABA cocrystal, the TG–DTA curves show that it is thermally stable up to 200 °C, which is between the thermal stability of the drug and the coformer. The TG curves also show four mass loss steps, corresponding to endothermic and exothermic events in the DTA curves, attributed to the thermal decomposition of the cocrystal. The first step between 200 and 280 °C is attributed to the thermal decomposition of the cocrystal with partial release of the coformer ($\Delta m_{Calc.} = 29.1\%$, $\Delta m_{TG} = 27.8\%$). This difference of 1.3% between the calculated and experimental values is attributed to partial thermal degradation of PABA with the formation of carbonaceous residue, as observed in the TG–DTA curves of the isolated coformer. The other three mass loss steps, corresponding to endothermic and exothermic events in the DTA curve, are attributed to the thermal degradation of the remaining drug.

The DSC curves show three thermal events: the first endothermic peak at 212 °C corresponding to the incongruent fusion of the samples, the second peak at 230° C corresponding to partial volatilization of the PABA and the third event, a very subtle exotherm around 230–245 °C,

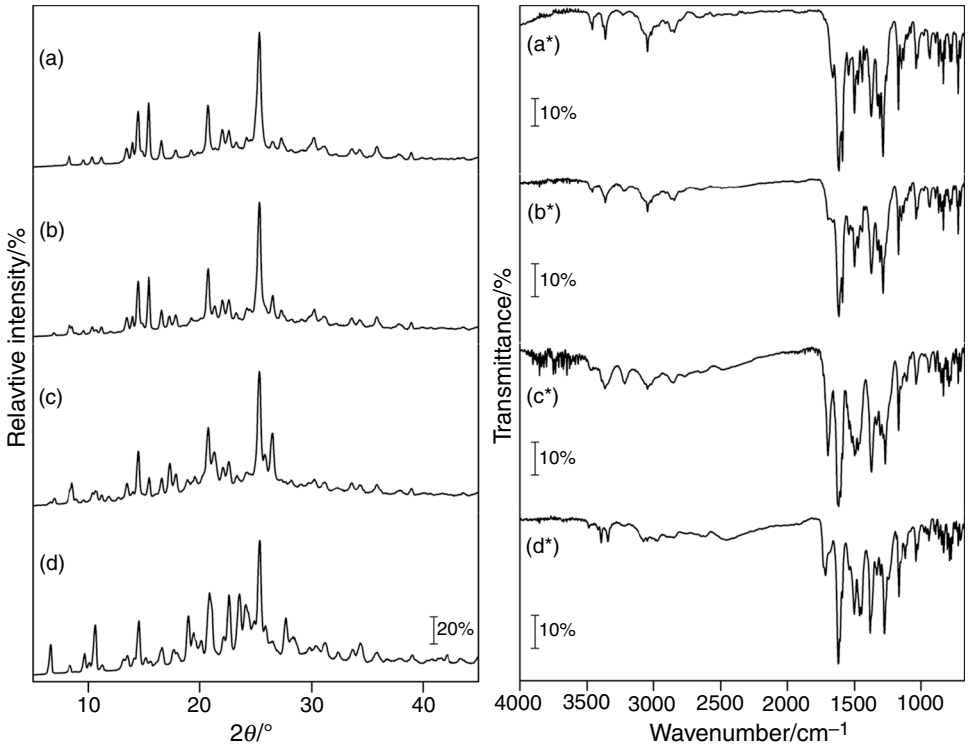

Fig. 8 PXRD diffractograms (**a**, **b**, and **c**) and FTIR spectra (**a***, **b*** and **c***) of the CIP–PABA/NG (15 Hz) systems at 25 °C (**a**, **a***), heated up to 100 °C (**b**, **b***), 125 °C (**c**, **c***) and 175 °C (**d**, **d***)

corresponding to crystallization of the remaining CIP, as can also be observed in the DSC-Microscopy micrographs (Fig. S3, supplementary material) and in the video (supplementary material). In addition, the systems obtained by the NG method show a third exothermic peak at 132 °C in the DSC curve, which was investigated by PXRD and FTIR, and the results will be presented further below.

The thermal behavior characteristic of these systems suggests the formation of CIP–PABA cocrystals in all the synthesis conditions (NG and LAG), although the diffraction and spectroscopic data show that this occurs only for the systems synthesized by the LAG method. These differences between the thermal and spectroscopic data are related to the exothermic event observed in the DSC curves of the systems obtained by the NG method.

Study of the exothermic events in the DSC curves

The PXRD diffractograms and FTIR spectra of the heated CIP–PABA/NG (15 Hz) physical mixture are presented in Fig. 8a, b, respectively.

These data show that the heating causes changes in PXRD diffractograms and FTIR spectra, leading to the appearance of diffraction peaks and FTIR bands corresponding to cocrystal formation. These changes occur drastically and are completed after the exothermic event in the DSC curve, promoting the complete formation of the cocrystal, since the diffraction and spectral pattern become the same as the cocrystals obtained by the LAG method. Therefore, these

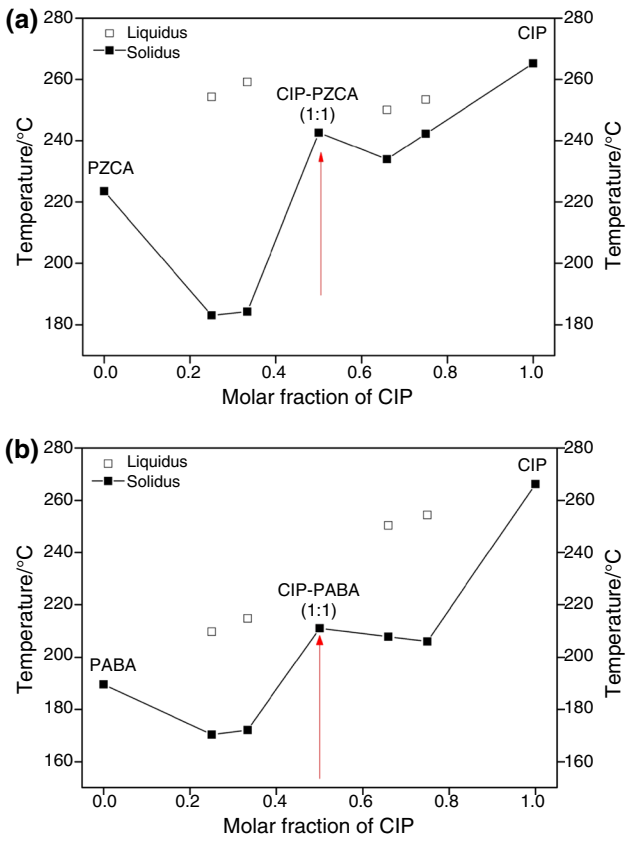

Fig. 9 Binary phase diagrams of CIP–PZCA (**a**) and CIP–PABA (**b**) systems

results suggest that the heating promotes the cocrystallization of the physical mixture, as already reported [49].

Binary phase diagrams

The binary phase diagrams constructed from the data of the DSC curves (Figs. S4 and S5, supplementary material) are shown in Fig. 9. These diagrams are W-shaped, characteristic of cocrystals [2, 51, 52], confirming the formation of the CIP–PZCA and CIP–PABA cocrystals in the ideal stoichiometry of 1:1 (API/coformer), since the molar fraction 0.5 represents the center point of the "*W*."

Conclusions

Cocrystallization has become an important approach to improve physicochemical properties of non-ionic compounds, such as the case of ciprofloxacin in its zwitterionic form. Following these lines, here the successful synthesis of cocrystals of ciprofloxacin with pyrazinoic acid and *p*-aminobenzoic acid by the mechanochemical method was reported, both with and without the use of solvent.

Via FTIR spectroscopy, PXRD, TG–DTA, DSC and DSC-Microscopy, it is demonstrated that both the LAG and NG approaches are efficient for the synthesis of CIP–PZCA cocrystals, although different polymorphs can be obtained. For the synthesis of the CIP–PABA cocrystals, the addition of solvent provided more efficiency, and it was not possible to obtain it by the NG method. Moreover, the binary phase diagrams indicate that 1:1 is the ideal stoichiometry for the cocrystal formation in both CIP–PZCA and CIP–PABA systems.

Finally, the thermoanalytical techniques are fundamental in the study and characterization of these multicomponent solids, since they provided information on composition, thermal stability, melting temperature and enthalpy, thermal decomposition profile, detection of crystallization processes for the CIP–PZCA cocrystal and polymorphic transition to CIP–PABA cocrystals.

Acknowledgements The authors thank CPID/CDMF, FAPESP (grant Nos. 2013/09022-7, 2017/14936-9, 2018/12463-9 and 2018/24378-6), CNPq (grant No. 141829/2017-6) and CAPES (grant No. 001) foundations (Brazil) for financial support.

References

1. Kawabata Y, Wada K, Nakatani M, Yamada S, Onoue S. Formulation design for poorly water-soluble drugs based on biopharmaceutics classification system: basic approaches and practical applications. Int J Pharm. 2011;420:1–10.
2. Sathisaran I, Dalvi S. Engineering cocrystals of poorly water-soluble drugs to enhance dissolution in aqueous medium. Pharmaceutics. 2018;10:108–82.
3. Cerreia Vioglio P, Chierotti MR, Gobetto R. Pharmaceutical aspects of salt and cocrystal forms of APIs and characterization challenges. Adv Drug Deliv Rev. 2017;117:86–110.
4. Aakeröy CB, Grommet AB, Desper J. Co-crystal screening of diclofenac. Pharmaceutics. 2011;3:601–14.
5. Lin HL, Zhang GC, Hsu PC, Lin SY. A portable fiber-optic Raman analyzer for fast real-time screening and identifying cocrystal formation of drug-coformer via grinding process. Microchem J. 2013;110:15–20.
6. Rajput L, Sanphui P, Desiraju GR. New solid forms of the anti-HIV drug etravirine: salts, cocrystals, and solubility. Cryst Growth Des. 2013;13:3681–90.
7. Jie Lu. Crystallization and transformation of pharmaceutical solid forms. Afr J Pharm Pharmacol. 2012;6:581–91.
8. Shevchenko A, Bimbo LM, Miroshnyk I, Haarala J, Jelínková K, Syrjänen K, et al. A new cocrystal and salts of itraconazole: comparison of solid-state properties, stability and dissolution behavior. Int J Pharm. 2012;436:403–9.
9. Rocha ABO, Kuminek G, Machado TC, Rosa J, Rauber GS, Borba PA, et al. Cocristais: uma estratégia promissora na área farmacêutica. Quim Nova. 2016;39:1112–25.
10. Brittain HG. Cocrystal Systems of pharmaceutical interest: 2010. Cryst Growth Des. 2012;12:1046–54.
11. Braga D, Maini L, Grepioni F. Mechanochemical preparation of co-crystals. Chem Soc Rev. 2013;42:7638–48.
12. Kotbantao G, Charoenchaitrakool M. Processing of ketoconazole–4-aminobenzoic acid cocrystals using dense CO_2 as an antisolvent. J CO2 Util. 2017;17:213–9.
13. Osonwa UE, Ugochukwu JI, Ajaegbu EE, Chukwu KI, Azevedo RB, Esimone CO. Enhancement of antibacterial activity of ciprofloxacin hydrochloride by complexation with sodium cholate. Bull Fac Pharm Cairo Univ. 2017;55:233–7.
14. Cazedey ECL, Salgado HRN. Spectrophotometric determination of ciprofloxacin hydrochloride in ophthalmic solution. Adv Anal Chem. 2012;2:74–9.
15. Mesallati H, Mugheirbi NA, Tajber L. Two faces of ciprofloxacin: investigation of proton transfer in solid state transformations. Cryst Growth Des. 2016;16:6574–85.
16. Yi K, Wang D, Qi Y, Li X, Chen H, Sun J, et al. Effect of ciprofloxacin on biological nitrogen and phosphorus removal from wastewater. Sci Total Environ. 2017;605–606:368–75.
17. Surov AO, Manin AN, Voronin AP, Drozd KV, Simagina AA, Churakov AV, et al. Pharmaceutical salts of ciprofloxacin with dicarboxylic acids. Eur J Pharm Sci. 2015;77:112–21.
18. Reddy JS, Ganesh SV, Nagalapalli R, Dandela R, Solomon KA, Kumar KA, et al. Fluoroquinolone salts with carboxylic acids. J Pharm Sci. 2011;100:3160–76.
19. Almeida AC, Torquetti C, Ferreira PO, Fernandes RP, Santos EC, Kogawa AC, Caires FJ. Cocrystals of ciprofloxacin with nicotinic and isonicotinic acids: mechanochemical synthesis, characterization, thermal and solubility study. Thermochim. Acta. 2019. https://doi.org/10.1016/j.tca.2019.178346.
20. Pinto Vitorino G, Sperandeo NR, Caira MR, Mazzieri MR. A supramolecular assembly formed by heteroassociation of ciprofloxacin and norfloxacin in the solid state: co-crystal synthesis and characterization. Cryst Growth Des. 2013;13:1050–8.
21. Martínez-Alejo JM, Domínguez-Chávez JG, Rivera-Islas J, Herrera-Ruiz D, Höpfl H, Morales-Rojas H, et al. A twist in cocrystals of salts: changes in packing and chloride coordination lead to opposite trends in the biopharmaceutical performance of fluoroquinolone hydrochloride cocrystals. Cryst Growth Des. 2014;14:3078–95.

22. Zhang Y-X, Wang L-Y, Dai J-K, Liu F, Li Y-T, Wu Z-Y, et al. The comparative study of cocrystal/salt in simultaneously improving solubility and permeability of acetazolamide. J Mol Struct. 2019;1184:225–32.
23. Arenas-García JI, Herrera-Ruiz D, Morales-Rojas H, Höpfl H. Interrelation of the dissolution behavior and solid-state features of acetazolamide cocrystals. Eur J Pharm Sci. 2017;96:299–308.
24. Qiao N, Li M, Schlindwein W, Malek N, Davies A, Trappitt G. Pharmaceutical cocrystals: an overview. Int J Pharm. 2011;419:1–11.
25. Thakuria R, Delori A, Jones W, Lipert MP, Roy L, Rodríguez-Hornedo N. Pharmaceutical cocrystals and poorly soluble drugs. Int J Pharm. 2013;453:101–25.
26. Chen J, Sarma B, Evans JMB, Myerson AS. Pharmaceutical crystallization. Cryst Growth Des. 2011;11:887–95.
27. Kirillov AM, Shul'pin GB. Pyrazinecarboxylic acid and analogs: highly efficient co-catalysts in the metal–complex-catalyzed oxidation of organic compounds. Coord Chem Rev. 2013;257:732–54.
28. Miniyar PB, Mokale SN, Makhija SJ. Design and synthesis of 5-methylpyrazine-2-carbohydrazide derivatives: a new antitubercular scaffold. Arab J Chem. 2017;10:41–6.
29. Barszcz B, Masternak J, Hodorowicz M, Jabłońska-Wawrzycka A. Cadmium(II) and calcium(II) complexes with N, O-bidentate ligands derived from pyrazinecarboxylic acid. J Therm Anal Calorim. 2012;108:971–8.
30. Etaiw SEH, El-bendary MM. Crystal structure, characterization and catalytic activities of Cu(II) coordination complexes with 8-hydroxyquinoline and pyrazine-2-carboxylic acid. Appl Organomet Chem. 2017;e4213:1–14.
31. Drozd KV, Arkhipov SG, Boldyreva EV, Perlovich GL. Crystal structure of a 1:1 salt of 4-aminobenzoic acid (Vitamin B 10) with pyrazinoic acid. Acta Crystallogr Sect E Crystallogr Commun. 2018;74:1923–7.
32. Prasad KD, Cherukuvada S, Ganduri R, Stephen LD, Perumalla S, Guru Row TN. Differential cocrystallization behavior of isomeric pyridine carboxamides toward antitubercular drug pyrazinoic acid. Cryst Growth Des. 2015;15:858–66.
33. Teixeira JA, Nunes WDG, Colman TAD, do Nascimento ALC, Caires FJ, Campos FX, et al. Thermal and spectroscopic study to investigate *p*-aminobenzoic acid, sodium *p*-aminobenzoate and its compounds with some lighter trivalent lanthanides. Thermochim Acta. 2016;624:59–68.
34. Akberova SI. New biological properties of *p*-aminobenzoic acid. Biol Bull. 2002;29:390–3.
35. Li Y, Tang L-P, Zhou W, Wang X-R. Fabrication of intercalated *p*-aminobenzoic acid into Zn–Ti layered double hydroxide and its application as UV absorbent. Chin Chem Lett. 2016;27:1495–9.
36. Patel HM, Bhardwaj V, Sharma P, Noolvi MN, Lohan S, Bansal S, et al. Quinoxaline-PABA bipartite hybrid derivatization approach: design and search for antimicrobial agents. J Mol Struct. 2019;1184:562–8.
37. Li Z, Matzger AJ. Influence of coformer stoichiometric ratio on pharmaceutical cocrystal dissolution: three cocrystals of carbamazepine/4-aminobenzoic acid. Mol Pharm. 2016;13:990–5.
38. Cherukuvada S, Babu NJ, Nangia A. Nitrofurantoin–*p*-aminobenzoic acid cocrystal: hydration stability and dissolution rate studies. J Pharm Sci. 2011;100:3233–44.
39. Friščić T, Childs SL, Rizvi SAA, Jones W. The role of solvent in mechanochemical and sonochemical cocrystal formation: a solubility-based approach for predicting cocrystallisation outcome. CrystEngComm. 2009;11:418–26.
40. Cortesão AM, Henriques JG, Castro RAE, Maria TMR, Canotilho J, Eusébio MES. Binary phase diagrams of pyridinecarboxamide isomers. J Therm Anal Calorim. 2017;130:1727–33.
41. Descamps M, Willart JF. Perspectives on the amorphisation/milling relationship in pharmaceutical materials. Adv Drug Deliv Rev. 2016;100:51–66.
42. Hasa D, Miniussi E, Jones W. Mechanochemical synthesis of multicomponent crystals: one liquid for one polymorph? A myth to dispel. Cryst Growth Des. 2016;16:4582–8.
43. Cinčić D, Brekalo I, Kaitner B. Solvent-free polymorphism control in a covalent mechanochemical reaction. Cryst Growth Des. 2012;12:44–8.
44. Choi JM, Park K, Lee B, Jeong D, Dindulkar SD, Choi Y, et al. Solubility and bioavailability enhancement of ciprofloxacin by induced oval-shaped mono-6-deoxy-6-aminoethylamino-β-cyclodextrin. Carbohydr Polym. 2017;163:118–28.
45. Wixtrom A, Buhler J, Abdel-Fattah T. Mechanochemical synthesis of two polymorphs of the tetrathiafulvalene–chloranil charge transfer salt: an experiment for organic chemistry. J Chem Educ. 2014;91:1232–5.
46. Fischer F, Heidrich A, Greiser S, Benemann S, Rademann K, Emmerling F. Polymorphism of mechanochemically synthesized cocrystals: a case study. Cryst Growth Des. 2016;16:1701–7.
47. Kendall DN. Identification of polymorphic forms of crystals by infrared spectroscopy. Anal Chem. 1953;25:382–9.
48. Giron D. Investigations of polymorphism and pseudo-polymorphism in pharmaceuticals by combined thermoanalytical techniques. J Therm Anal Calorim. 2001;64:37–60.
49. Lin H-L, Huang Y-T, Lin S-Y. Spectroscopic and thermal approaches to investigate the formation mechanism of piroxicam–saccharin co-crystal induced by liquid-assisted grinding or thermal stress. J Therm Anal Calorim. 2016;123:2345–56.
50. Tantishaiyakul V, Dokmaisrijan S, Sangfai T, Hirun N, Li L, Juntarapet S, et al. Investigation of the efficiency of gelation of melamine with the positional isomers of aminobenzoic acid. Colloids Surf A Physicochem Eng Asp. 2014;446:118–26.
51. Cherukuvada S, Guru Row TN. Comprehending the formation of eutectics and cocrystals in terms of design and their structural interrelationships. Cryst Growth Des. 2014;14:4187–98.
52. Li H-R, Shu Y-J, Song C, Chen L, Xu R-J, Ju X-H. The smart precursors of energetic–energetic cocrystals from eutectic precursors. Chin Chem Lett. 2014;25:783–6.